

Unambiguous tracking of protein phosphorylation by fast, high-resolution FOSY NMR.

Dmitry M. Lesovoy,[‡] Panagiota S. Georgoulia,[‡] Tammo Diercks, Irena Matečko-Burmann, Björn M. Burmann, Eduard V. Bocharov, Wolfgang Bermel, and Vladislav Y. Orekhov*.

ABSTRACT: Phosphorylation is a prototypical example of post-translational modifications (PTMs) that dynamically modulates protein function, and its dysregulation is often implicated in disease. NMR provides atom-level information on exact positions and time course of PTM's under nearly physiological conditions, even inside living cells, but initially requires an unambiguous assignment of NMR signals to individual atoms in the affected protein regions. Yet, existing methods for this task are based on a global, hence, costly and tedious NMR signal assignment that may often fail, especially for large intrinsically disordered proteins (IDPs). Here we introduce a sensitive and robust method to rapidly obtain only the relevant local NMR signal assignment, based on a suite of Focused SpectroscopyY (FOSY) experiments that employ the long overlooked concept of selective polarisation transfer (SPT). We then demonstrate the efficiency of the FOSY by fast and reliable NMR signal assignment of two phosphorylation sites, Ser⁴⁰⁴ and Ser⁴⁰⁹ of proline-dependent glycogen synthase kinase 3 beta (GSK3 β) in human hTau40, an IDP of 441 residues. Unprecedented spectral resolution in FOSY spectra allowed us to unambiguously show for the first time that GSK3 β can phosphorylate Ser⁴⁰⁹ without priming by other protein kinases. The new approach will benefit NMR studies of other PTMs and protein hotspots in general, including sites involved in molecular interactions and conformational changes.

Post-translational modifications (PTMs) constitute an additional level of complexity modulating protein function, of which phosphorylation is the best studied signalling switch, abundant and essential in the regulation of intrinsically disordered proteins (IDPs).¹⁻³ Phosphorylation is conventionally detected and quantified by mass spectrometry, then validated by mutagenesis or antibody binding assays. This procedure is expensive, time-consuming, and often fraught with problems especially for highly charged phosphopeptides, repetitive sequences, and proximal modification sites, all of which are hallmarks of IDPs.⁴⁻⁵ To address these difficulties, time-resolved heteronuclear NMR methods have been developed allowing also to derive the reaction kinetics.⁶⁻¹⁰ Yet, these require prior NMR signal assignment for the entire protein, which so far is obtained from a suite of multi-dimensional experiments¹¹⁻¹⁶ with often limited sensitivity, after several days of measurements and sophisticated analysis to resolve assignment ambiguities that may prove impossible in highly crowded spectral regions.¹⁷ Thus, a fast, simple, and reliable NMR approach for tracking PTMs, like phosphorylation, would provide a tremendous advantage in elucidating their role within signalling proteins at the atomic resolution.¹⁸⁻²⁰

To address this need, we introduce here Focused SpectroscopyY (FOSY) as a fast *de novo* assignment strategy for localised structural hotspots based on a set of frequency-selective experiments combining the ultra-high resolution of up to six- or seven-dimensional (6D, 7D) spectra with the sensitivity, speed, and simplicity of 2D spectra. The novel approach enables the direct assignment of PTM sites within IDPs from a

minimal set of fast and easy to analyse NMR experiments elucidating their local sequential surroundings.

Central to our method for focussing onto the few residues affected by PTMs and solving the spectral resolution problem in only two dimensions, is the use of frequency selective polarisation transfer (SPT) to single out one coupled nuclear spin system at a time and with efficiency and versatility higher than the one achievable by traditional broadband experiments.²¹⁻²² While optimising sensitivity, multiple selection of known frequencies along a chosen spin system minimises spectral complexity and makes their lengthy sampling in further indirect dimensions redundant. While SPT is a known technique with several clear advantages, its use has so far been limited to isolated two-spin systems²³⁻²⁵ such as the ¹H-¹⁵N amide groups, allowing a reduction by just two spectral dimensions. Thus, a 6D could be cut down to a 4D experiment that would still take impractically long to measure for each selected residue at a time. Here we introduce the frequency Selective and Spin-State Selective Polarisation Transfer (S⁴PT) as a generalized SPT approach for coupled multi-spin systems, as found in isotopically labelled amino acids, that allows eliminating several pertaining spectral dimensions and avoiding competing magnetisation transfer *via* passive spin couplings. The novel 2D FOSY experiments (Figure 1), yield a spectral resolution dispersion comparable to the 6D HNCOCANH¹¹ and 7D HNCOCACBNH experiments, yet with far superior sensitivity and ease of analysis.

As a showcase application for the proposed FOSY approach to monitor PTMs in IDPs, we identify sites phosphorylated *in vitro* by proline-dependent glycogen synthase kinase 3 beta

(GSK3 β)²⁶ in the representative 441-residue long hTau40 protein, which comprises 80 serines and threonines as putative phosphorylation sites. Abnormal hTau hyper-phosphorylation is directly linked to dysregulation and possibly aggregation that characterises neurodegenerative tauopathies, such as Alzheimer's disease.²⁷⁻³¹ As a first step of our strategy (outlined in Figure 2a) we searched for spectral changes from GSK3 β -mediated phosphorylation of Tau in the most sensitive and well-dispersed 3D HNCO spectrum, which revealed several shifted or newly appearing signals for pTau (peaks a–g in Figure S4). Due to the proline and glycine rich character of IDPs, we assembled a list of peptide stretches from the hTau sequence that conform with the general sequence motif (P/G)-Xⁿ-p(S/T)-Xⁿ-(P/G), where X \neq Pro,Gly. This list can be further curated by exploiting the reported phosphorylation sites in the literature or known kinase consensus sequence motifs (Table S1). The first step of the process was concluded by acquiring a pair of complementary 2D proline selective experiments³² to identify the residues following (PX-) or preceding (-XP) prolines (Figure S5).

To start the FOSY assignment we focus on the peak 0 in Figure 2b, which appears in the 3D HNCO spectrum after Tau phosphorylation (peak 'a' in Figure S4) and likely corresponds to a phosphorylated serine (pS) or threonine (pT). Inspection of the two Pro-selective experiments reveals that this new signal derives from a pS or pT preceding a proline (i.e., an p(S/T)P motif, Table S1). A pair of new 2D FOSY hncoc(CA)NH and hncoc(CA)(N)H experiments (Figure 1) for signal 0 were recorded by selecting its exact $^1\text{H}^{\text{N},0}$, $^{15}\text{N}^{\text{H},0}$, $^{13}\text{C}^{\text{O},-1}$ frequencies known from the 3D HNCO spectrum, which yielded the $^{15}\text{N}^{\text{H},-1}$, $^1\text{H}^{\text{N},-1}$, and $^{13}\text{C}^{\text{A},-1}$ frequencies of the preceding residue. This connects signal 0 to the preceding X-type residue signal -1 in Figure 2b, resulting in an -Xp(S/T)P motif. We continue walking to peak -2 using the $^{15}\text{N}^{\text{H},-1}$, $^1\text{H}^{\text{N},-1}$ and the $^{13}\text{C}^{\text{O},-2}$ frequencies (the latter again derived from the initially recorded 3D HNCO) and further on until we reach a PX-type residue or, as in this case, a GX-type residue identified by the characteristic glycine chemical shifts of $^{15}\text{N}^{\text{H}}$ and $^{13}\text{C}^{\text{A}}$ and the negative intensity due to constant-time evolution of the $^{13}\text{C}^{\text{A},-1}$ chemical shift. We thus identify a -GXp(S/T)P motif that has only two possible matches in the hTau sequence, G¹⁹⁶YSS¹⁹⁹P and G⁴⁰¹DTS⁴⁰⁴P, respectively.

To resolve this ambiguity or, in case of several observed peaks in the 2D hncoc(CA)NH and hncoc(CA)(N)H spectra due to overlap of the selected initial fixed frequencies (e.g. fixing peak -2 provides peaks -3 and -3*), we recorded a complementary 2D FOSY hncocac(N)H experiment (Figure 1) with five fixed frequencies ($^1\text{H}^{\text{N},0}$, $^{15}\text{N}^{\text{H},0}$, $^{13}\text{C}^{\text{O},-1}$, $^{13}\text{C}^{\text{A},-1}$, $^{13}\text{C}^{\text{B},-1}$) to determine the type of the preceding residue. The $^{13}\text{C}^{\text{B},-1}$ frequency is taken from the residue-type-specific chemical shifts for random coil.³³⁻³⁴ This experiment, providing a signal only if the correct $^{13}\text{C}^{\text{B},-1}$ frequency is hit by frequency selective decoupling³⁵⁻³⁶ and no signal otherwise, confirms Thr (but not Ser) for peak -1 and thereby reveals the GXTp(S/T)P sequence motif. This unambiguously maps onto the hTau primary sequence and thereby assigns peak 0 to pS⁴⁰⁴.

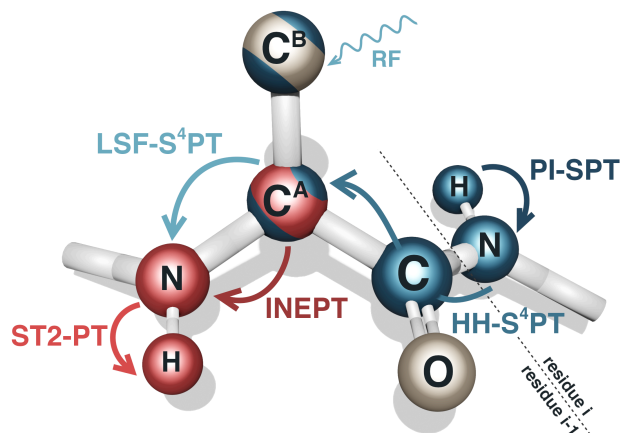


Figure 1. Scheme of the magnetization pathway in the 2D FOSY hncoc(CA)NH, hncoc(CA)(N)H, and hncocac(N)H experiments (see Supplementary Figure S1). Selective (PI-SPT, HH-S⁴PT, LSF-S⁴PT) and broadband (INEPT, ST2-PT^{32, 37}) polarisation transfer steps are annotated and color-coded in blue and red respectively; atoms with the “fixed” and “traditionally” sampled nuclei are also shown as blue and red balls; optionally “fixed” atoms are stripe edged. In a di-peptide unit with residues at the positions i and $i-1$, the magnetization flow is started at $^1\text{H}^{\text{N},i}$ and detected at $^1\text{H}^{\text{N},i-1}$. The frequencies of $^1\text{H}^{\text{N},i}$, $^{15}\text{N}^{\text{H},i}$, and $^{13}\text{C}^{\text{O},i-1}$ are known, e.g. from an HNCO experiment, and fixed with high precision, whereas the remaining frequencies of $^{13}\text{C}^{\text{A},i-1}$, $^{15}\text{N}^{\text{H},i-1}$, and $^1\text{H}^{\text{N},i-1}$ are sampled in the traditional way. In the 2D hncocac(N)H also $^{13}\text{C}^{\text{A},i-1}$ and $^{13}\text{C}^{\text{B},i-1}$ are fixed. As the cornerstone of the FOSY experiments, we introduce a method of frequency selective and spin-state selective polarization transfer S⁴PT that allows to organize a continuous SPT that can be optimized and tailored to the properties of a specific multi-spin system, such as relaxation²¹, conformational²³⁻²⁴ and chemical²² exchange, amino acid type, etc. The experiments start with the selective polarisation transfer by the population inversion of the TROSY³⁷ component of the ^1H magnetization (PI-SPT). PI-SPT has the highest theoretically possible efficiency surpassing the methods available for the traditional non-selective experiments.²¹ Then, use of S⁴PT version of the selective heteronuclear Hartmann-Hahn provides sensitivity gain by shortening the transfer time of the two-spin magnetization $2H_z^i N_z^i$ obtained at the previous step to $^{13}\text{C}^{\text{A},i-1}$ atom as $2C_z^{A,i-1} C_z^{O,i-1}$. This HH-S⁴PT is transverse relaxation optimized³⁷ as it avoids any mixture of the slowly and fast relaxing ^{15}N coherence. Notably, while conventional non-selective experiments exploit only one of the two coherence components, SPT uses both for better sensitivity. Versatility of the HH-S⁴PT allows to prioritize either the highest spectral resolution on the frequency of $^{15}\text{N}^{\text{H},i}$ or the sensitivity by minimizing the relaxation losses. Subsequently, when $^{13}\text{C}^{\text{A},i-1}$ and $^{13}\text{C}^{\text{B},i-1}$ are fixed in the hncocac(N)H experiment, S⁴PT allows use of Longitudinal Single Field polarization transfer (LSF-SPT)³⁸ for magnetization transfer between $^{13}\text{C}^{\text{A},i-1}$ and $^{15}\text{N}^{\text{H},i-1}$ atoms as $C_z^{A,i-1} C_z^{O,i-1} \rightarrow C_x^{A,i-1} N_z^{i-1}$ with concurrent selective decoupling of $^{13}\text{C}^{\text{B},i-1}$. Finally, we note that the FOSY experiments benefit from the longitudinal relaxation optimization¹¹ by preserving both water and aliphatic proton polarization at thermal equilibrium

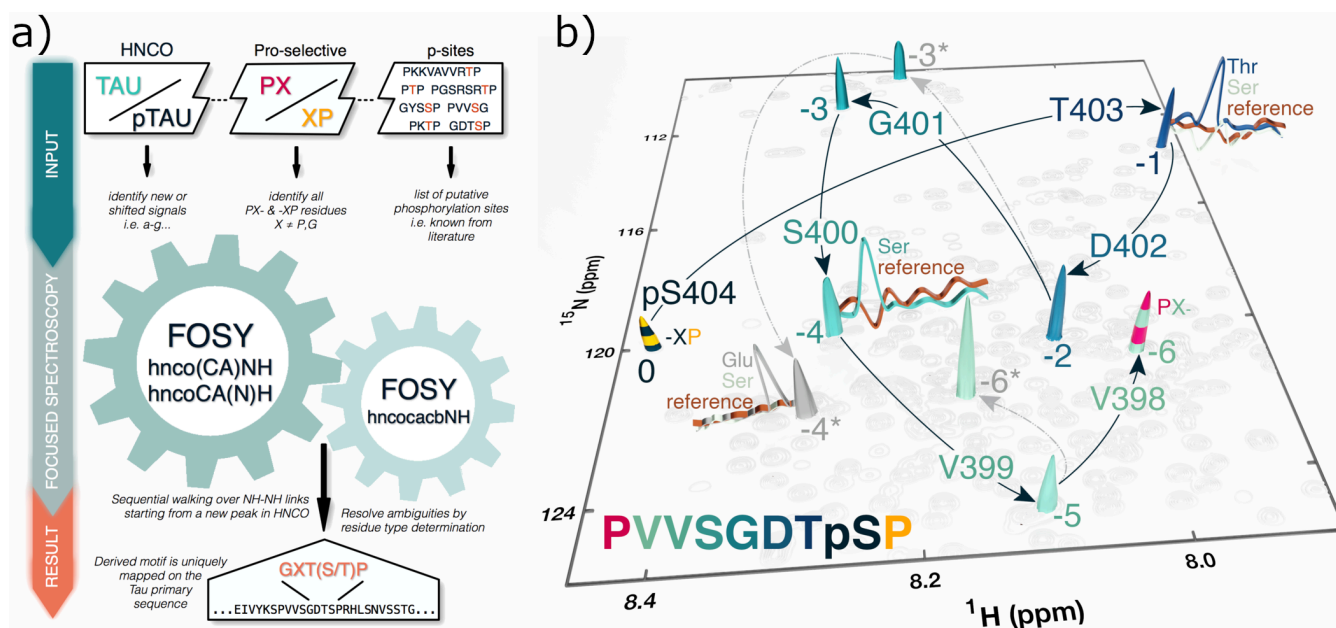


Figure 2. Schematic outline (a) of the FOSY assignment strategy and (b) its application to assign a putative phosphorylation site at the newly appeared signal 0 in p-hTau40. This peak was identified as XP-type in the proline-selective experiment. Sequential walk (black arrows) over the NH-NH links is traced out by successive iterations of the 2D FOSY-hnco(CA)NH experiments. The peaks are numbered and gradually color-coded according to their “step” number, as indicated in the peptide sequence in the lower left corner. Alternative sequential $i-1$ signals appearing due to overlap of their parent i signals in the HNCO spectrum are asterisked and connected by dashed grey arrows. To resolve eventual ambiguities, alternative residue types were tested with the 2D FOSY-hncocacabNH experiment, that produces a signal (inserted as 1D ^1H projections) only if the correct $^{13}\text{C}^{\beta-1}$ is selected. The derived PXXSGXTp(S/T)P motif unambiguously assigns signal 0 to pS⁴⁰⁴.

Similarly, using hncocacabNH experiment, only peak -3 out of the two Gly peaks -3, -3* in Figure 2b, has a preceding Ser (-4) matching the sequence whereas -3* has a preceding Glu (peak -4*). Subsequent walking identifies peak -5 as non PX-type residue and peak -6 (but not -6*) as PX-type, concluding and further validating the mapping of the pS⁴⁰⁴ site on the unique PXXSGXTp(S/T)P peptide sequence motif. The minimal procedure for unambiguous sequence specific identification of the pS⁴⁰⁴ site required nine 2D FOSY experiments (Figure S5), specifically three hnco(CA)NH and three hncoCA(N)H spectra for the sequential walk and three hncocacabNH to identify the residue type in position -1, amounting to a total experimental time of less than two hours. The 2D spectra contained only a single or very few peaks, allowing straightforward analysis in real time. In the Supporting Information (Figure S6), we present the identification of the second phosphorylation site pS⁴⁰⁹, which together with pS⁴⁰⁴, explains all newly appeared or shifted signals in the HNCO spectrum of pTau. Notably, while the proline-dependent pS⁴⁰⁴ site was already known from prior studies,^{26, 39} only the extreme spectral simplification and dispersion afforded by our new FOSY approach allowed the additional detection of S⁴⁰⁹ phosphorylation by GSK3 β . Although phosphorylation of this residue was previously suggested to occur in the pre-neurofibrillar tangle state of hTau,³⁰ it could not yet be unambiguously shown that it can be catalysed by GSK3 β without priming by other protein kinases.⁴⁰

We have demonstrated the *de novo* identification of phosphorylation sites in IDPs through the application of the fast and

robust new FOSY NMR approach. The proposed strategy does not rely on known assignment and can be readily applied irrespective of prior knowledge of the modifiable sites. A hallmark of the approach is the focus on only small relevant parts of the protein, which is much faster and versatile than the traditional global assignment, where the efforts are bound to the full size of the system. The analysis is straightforward due to the extreme simplicity of the 2D FOSY spectra that still capture the enormous resolution and dispersion of complex 6D and 7D experiments.

Therefore, the great benefits and versatility of frequency selective NMR approaches, as demonstrated in the presented proof of concept study on IDP phosphorylation, should be generalizable and will make a multitude of biomolecular hotspots newly tractable by NMR.

AUTHOR INFORMATION

Corresponding Author

Vladislav Y. Orekhov - Department of Chemistry and Molecular Biology, University of Gothenburg, Box 465, 405 30, Gothenburg, Sweden; Swedish NMR Centre, University of Gothenburg, Box 465, 405 30, Gothenburg, Sweden. ORCID: 0000-0002-7892-6896
Email: vladislav.orekhov@nmr.gu.se

Author Contributions

‡These authors contributed equally.

Authors

Dmitry M. Lesovoy - Department of Structural Biology, Shemyakin-Ovchinnikov Institute of Bioorganic Chemistry RAS, 117997, Moscow, Russia; Research Center for Molecular Mechanisms of Aging and Age-related Diseases, Moscow Institute of Physics and Technology (State University), 141700 Dolgoprudny, Russia. ORCID: 0000-0002-9130-715X

Panagiota S. Georgoulia - Department of Chemistry and Molecular Biology, University of Gothenburg, Box 465, 405 30, Gothenburg, Sweden ORCID: 0000-0003-4573-8052

Tammo Diercks – NMR Platform, CiC bioGUNE, Bld. 800, Parque Tecnológico de Bizkaia, 48160 Derio, Spain. ORCID: 0000-0002-5200-0905

Irena Matečko-Burmann - Department of Psychiatry and Neurochemistry, University of Gothenburg, 405 30 Gothenburg, Sweden; Wallenberg Centre for Molecular and Translational Medicine, University of Gothenburg, 405 30 Gothenburg, Sweden. ORCID: 0000-0001-8873-8381

Björn M. Burmann - Department of Chemistry and Molecular Biology, University of Gothenburg, Box 465, 405 30, Gothenburg, Sweden; Wallenberg Centre for Molecular and Translational Medicine, University of Gothenburg, 405 30 Gothenburg, Sweden. ORCID: 0000-0002-3135-7964

Eduard V. Bocharov - Department of Structural Biology, Shemyakin-Ovchinnikov Institute of Bioorganic Chemistry RAS, 117997, Moscow, Russia; Research Center for Molecular Mechanisms of Aging and Age-related Diseases, Moscow Institute of Physics and Technology (State University), 141700 Dolgoprudny, Russia. ORCID: 0000-0002-3635-1609

Wolfgang Bermel - Bruker BioSpin GmbH, Silberstreife, 76287 Rheinstetten, Germany.

Funding Sources

The work was sponsored by Swedish Research Council to V.Y.O. (grant 2019-03561) and Russian Science Foundation to D.M.L. and E.V.B. (grant 19-74-30014, in part of NMR pulse sequence design). B.M.B. gratefully acknowledges funding from the Knut och Alice Wallenberg Foundation through the Wallenberg Centre for Molecular and Translational Medicine, University of Gothenburg, Sweden.

Notes

The presented pulse sequences for Bruker Avance spectrometers are available on request from the authors.

ACKNOWLEDGMENT

The authors thank Dr. Ilya S. Kuprov for helpful discussions.

REFERENCES

- Walsh, C. T.; Garneau-Tsodikova, S.; Gatto Jr, G. J., Protein posttranslational modifications: the chemistry of proteome diversifications. *Angew. Chem. Int. Ed.* **2005**, *44* (45), 7342-7372.
- Bah, A.; Forman-Kay, J. D., Modulation of Intrinsically Disordered Protein Function by Post-translational Modifications. *J. Biol. Chem.* **2016**, *291* (13), 6696-705.
- Boeynaems, S.; Alberti, S.; Fawzi, N. L.; Mittag, T.; Polymeridou, M.; Rousseau, F.; Schymkowitz, J.; Shorter, J.; Wolozin, B.; Van Den Bosch, L., Protein phase separation: a new phase in cell biology. *Trends Cell Biol.* **2018**, *28* (6), 420-435.
- Mitra, G., Emerging Role of Mass Spectrometry-Based Structural Proteomics in Elucidating Intrinsic Disorder in Proteins. *Proteomics* **2020**, 2000011.
- Mair, W.; Muntel, J.; Tepper, K.; Tang, S.; Biernat, J.; Seeley, W. W.; Kosik, K. S.; Mandelkow, E.; Steen, H.; Steen, J. A., FLEXITau: Quantifying Post-translational Modifications of Tau Protein in Vitro and in Human Disease. *Anal. Chem.* **2016**, *88* (7), 3704-14.
- Landrieu, I.; Lacosse, L.; Leroy, A.; Wieruszeski, J.-M.; Trivelli, X.; Sillen, A.; Sibille, N.; Schwalbe, H.; Saxena, K.; Langer, T., NMR analysis of a Tau phosphorylation pattern. *J. Am. Chem. Soc.* **2006**, *128* (11), 3575-3583.
- Theillet, F. X.; Rose, H. M.; Liokatis, S.; Binolfi, A.; Thongwichian, R.; Stuiver, M.; Selenko, P., Site-specific NMR mapping and time-resolved monitoring of serine and threonine phosphorylation in reconstituted kinase reactions and mammalian cell extracts. *Nat. Protoc.* **2013**, *8* (7), 1416-32.
- Mayzel, M.; Rosenlow, J.; Isaksson, L.; Orekhov, V. Y., Time-resolved multidimensional NMR with non-uniform sampling. *J. Biomol. NMR* **2014**, *58* (2), 129-39.
- Rosenlow, J.; Isaksson, L.; Mayzel, M.; Lengqvist, J.; Orekhov, V. Y., Tyrosine phosphorylation within the intrinsically disordered cytosolic domains of the B-cell receptor: an NMR-based structural analysis. *PLoS One* **2014**, *9* (4), e96199.
- Alik, A.; Bouguetoul, C.; Julien, M.; Bermel, W.; Ghouil, R.; Zinn-Justin, S.; Theillet, F. X., Sensitivity-Enhanced ¹³C-NMR Spectroscopy for Monitoring Multisite Phosphorylation at Physiological Temperature and pH. *Angew. Chem.* **2020**.
- Lescop, E.; Schanda, P.; Brutscher, B., A set of BEST triple-resonance experiments for time-optimized protein resonance assignment. *J. Magn. Reson.* **2007**, *187* (1), 163-169.
- Isaksson, L.; Mayzel, M.; Saline, M.; Pedersen, A.; Rosenlöv, J.; Brutscher, B.; Karlsson, B. G.; Orekhov, V. Y., Highly efficient NMR assignment of intrinsically disordered proteins: application to B- and T cell receptor domains. *PLoS One* **2013**, *8* (5), e62947.
- Moťáková, V.; Nováček, J.; Zawadzka-Kazimierczuk, A.; Kazimierczuk, K.; Židek, L.; Šanderová, H.; Krásný, L.; Koźmiński, W.; Sklenář, V., Strategy for complete NMR assignment of disordered proteins with highly repetitive sequences based on resolution-enhanced 5D experiments. *J. Biomol. NMR* **2010**, *48* (3), 169-177.
- Bermel, W.; Bertini, I.; Felli, I. C.; Gonnelli, L.; Koźmiński, W.; Piai, A.; Pierattelli, R.; Stanek, J., Speeding up sequence specific assignment of IDPs. *J. Biomol. NMR* **2012**, *53* (4), 293-301.
- Narayanan, R. L.; Dürr, U. H.; Bibow, S.; Biernat, J.; Mandelkow, E.; Zweckstetter, M., Automatic assignment of the intrinsically disordered protein Tau with 441-residues. *J. Am. Chem. Soc.* **2010**, *132* (34), 11906-11907.
- Pustovalova, Y.; Mayzel, M.; Orekhov, V. Y., XLSY: Extra-Large NMR Spectroscopy. *Angew. Chem.* **2018**, *130* (43), 14239-14241.
- Theillet, F. X.; Smet-Nocca, C.; Liokatis, S.; Thongwichian, R.; Kosten, J.; Yoon, M. K.; Kriwacki, R. W.; Landrieu, I.; Lippens, G.; Selenko, P., Cell signaling, post-translational protein modifications and NMR spectroscopy. *J. Biomol. NMR* **2012**, *54* (3), 217-36.

18. Bugge, K.; Brakti, I.; Fernandes, C. B.; Dreier, J. E.; Lundsgaard, J. E.; Olsen, J. G.; Skriver, K.; Kragelund, B. B., Interactions by disorder—a matter of context. *Front. Mol. Biosci.* **2020**, *7*.
19. Berlow, R. B.; Dyson, H. J.; Wright, P. E., Functional advantages of dynamic protein disorder. *FEBS Lett.* **2015**, *589* (19), 2433-2440.
20. Darling, A. L.; Uversky, V. N., Intrinsic disorder and posttranslational modifications: the darker side of the biological dark matter. *Front. genet.* **2018**, *9*, 158.
21. Khaneja, N.; Luy, B.; Glaser, S. J., Boundary of quantum evolution under decoherence. *PNAS* **2003**, *100* (23), 13162-13166.
22. Novakovic, M.; Kupče, Ě.; Oxenfarth, A.; Battistel, M. D.; Freedberg, D. I.; Schwalbe, H.; Frydman, L., Sensitivity enhancement of homonuclear multidimensional NMR correlations for labile sites in proteins, polysaccharides, and nucleic acids. *Nat. Commun* **2020**, *11* (1), 1-12.
23. Hansen, A. L.; Nikolova, E. N.; Casiano-Negroni, A.; Al-Hashimi, H. M., Extending the range of microsecond-to-millisecond chemical exchange detected in labeled and unlabeled nucleic acids by selective carbon R1ρ NMR spectroscopy. *J. Am. Chem. Soc.* **2009**, *131* (11), 3818-3819.
24. Korzhnev, D. M.; Orekhov, V. Y.; Kay, L. E., Off-resonance R1ρ NMR studies of exchange dynamics in proteins with low spin-lock fields: an application to a Fyn SH3 domain. *J. Am. Chem. Soc.* **2005**, *127* (2), 713-721.
25. Walinda, E.; Morimoto, D.; Shirakawa, M.; Sugase, K., F 1 F 2-selective NMR spectroscopy. *J. Biomol. NMR* **2017**, *68* (1), 41-52.
26. Godemann, R.; Biernat, J.; Mandelkow, E.; Mandelkow, E.-M., Phosphorylation of tau protein by recombinant GSK-3β: pronounced phosphorylation at select Ser/Thr-Pro motifs but no phosphorylation at Ser262 in the repeat domain. *FEBS Lett.* **1999**, *454* (1-2), 157-164.
27. Stoothoff, W. H.; Johnson, G. V., Tau phosphorylation: physiological and pathological consequences. *Biochim. Biophys. Acta* **2005**, *1739* (2-3), 280-97.
28. Hanger, D. P.; Anderton, B. H.; Noble, W., Tau phosphorylation: the therapeutic challenge for neurodegenerative disease. *Trends Mol. Med.* **2009**, *15* (3), 112-9.
29. Guo, T.; Noble, W.; Hanger, D. P., Roles of tau protein in health and disease. *Acta Neuropathol.* **2017**, *133* (5), 665-704.
30. Rankin, C. A.; Sun, Q.; Gamblin, T. C., Tau phosphorylation by GSK-3β promotes tangle-like filament morphology. *Mol. Neurodegener.* **2007**, *2*, 12.
31. Hernandez, F.; Gomez de Barreda, E.; Fuster-Matanzo, A.; Lucas, J. J.; Avila, J., GSK3: a possible link between beta amyloid peptide and tau protein. *Exp. Neurol.* **2010**, *223* (2), 322-5.
32. Solyom, Z.; Schwarten, M.; Geist, L.; Konrat, R.; Willbold, D.; Brutscher, B., BEST-TROSY experiments for time-efficient sequential resonance assignment of large disordered proteins. *J. Biomol. NMR* **2013**, *55* (4), 311-21.
33. Tamiola, K.; Acar, B.; Mulder, F. A., Sequence-specific random coil chemical shifts of intrinsically disordered proteins. *J. Am. Chem. Soc.* **2010**, *132* (51), 18000-18003.
34. Hendus-Altenburger, R.; Fernandes, C. B.; Bugge, K.; Kunze, M. B. A.; Boomsma, W.; Kragelund, B. B., Random coil chemical shifts for serine, threonine and tyrosine phosphorylation over a broad pH range. *J. Biomol. NMR* **2019**, *73* (12), 713-725.
35. Huth, J.; Bodenhausen, G., Suppression of passive scalar couplings in doubly selective coherence transfer. *J. Magn. Reson., Ser A* **1995**, *114* (1), 129-131.
36. Ritter, C.; Lühns, T.; Kwiatkowski, W.; Riek, R., 3d Trosy-Hnca Coded cb and Trosy-Hnca Coded co Experiments: Triple Resonance nmr Experiments With two Sequential Connectivity Pathways and High Sensitivity. *J. Biomol. NMR* **2004**, *28* (3), 289-294.
37. Pervushin, K. V.; Wider, G.; Wüthrich, K., Single transition-to-single transition polarization transfer (ST2-PT) in [15N, 1H]-TROSY. *J. Biomol. NMR* **1998**, *12* (2), 345-348.
38. Rey Castellanos, E. R.; Frueh, D. P.; Wist, J., Selective polarization transfer using a single rf field. *J. Chem. Phys.* **2008**, *129* (1), 07B602.
39. Leroy, A.; Landrieu, I.; Huvent, I.; Legrand, D.; Codeville, B.; Wieruszeski, J. M.; Lippens, G., Spectroscopic studies of GSK3{beta} phosphorylation of the neuronal tau protein and its interaction with the N-terminal domain of apolipoprotein E. *J. Biol. Chem.* **2010**, *285* (43), 33435-44.
40. Lippens, G.; Amniai, L.; Wieruszeski, J. M.; Sillen, A.; Leroy, A.; Landrieu, I., Towards understanding the phosphorylation code of tau. *Biochem. Soc. Trans.* **2012**, *40* (4), 698-703.

Supporting Information

Unambiguous tracking of protein phosphorylation by fast, high-resolution FOSY NMR.

Dmitry M. Lesovoy,[‡] Panagiota S. Georgoulia,[‡] Tammo Diercks, Irena Matečko-Burmann, Björn M. Burmann, Eduard V. Bocharov, Wolfgang Bermel, and Vladislav Y. Orekhov*

[‡] *These authors contributed equally.*

* Corresponding author. e-mail: vladislav.orekhov@nmr.gu.se

Selective Polarisation Transfer schemes

PI-SPT

For a heteronuclear IS two spin- $\frac{1}{2}$ system with mutual scalar J_{IS} coupling, I spin coherence produces an in-phase signal doublet with frequencies $\nu^I + J_{IS}/2$ and $\nu^I - J_{IS}/2$ as the coupled S spin may be aligned either parallel (S_α) or antiparallel (S_β) with the external magnetic field, respectively. An inversion pulse applied with high selectivity at the frequency $\nu^I - J_{IS}/2$ then creates γ_S enhanced anti-phase $2I_z S_z = I_z S_\alpha - I_z S_\beta$ magnetization. This scheme for magnetization transfer,^{1,2} which we abbreviate PI-SPT (Population Inversion for Selective Polarisation Transfer), is frequency selective for spin I and notably immune to any further (other than J_{IS}) passive scalar couplings of spin S. Furthermore, when the H_β TROSY polarisation component of the ^{15}N doublet is inverted by a CROP-shaped selective pulse, PI-SPT reaches the physical limit of efficiency for magnetization transfer³ in an amide HN spin system, surpassing all non-frequency selective PT schemes.

For the following section, we note that term $2I_z S_z$ can be also presented as $2I_z S_z = I_\alpha S_z - I_\beta S_z$, where $I_{\alpha/\beta}$ present single spin states of spin I. Both $I_\alpha S_z$ and $I_\beta S_z$ terms are directly used by the subsequent $S^4\text{PT}$ block without need for intermittent complete magnetization conversion of $2I_z S_z$ to spin S.

HH- $S^4\text{PT}$ - Heteronuclear Hartmann-Hahn (HH) frequency Selective and Spin-State Selective Polarisation Transfer ($S^4\text{PT}$)

In an isolated heteronuclear IS two-spin system with mutual J_{IS} coupling, selective I \rightarrow S Hartmann-Hahn polarization transfer⁴ (HH-SPT) can be achieved by simultaneous weak continuous wave (CW) irradiation at the exact ν^I and ν^S frequencies for a duration $\tau_{\text{CW}} = 1/J_{IS}$ and with identical $B_{1,I} = B_{1,S}$ field strengths

$$B_1 = \frac{J_{IS}\sqrt{4n^2-1}}{4} \quad [\text{S1}]$$

where $n = 1, 2, \dots$. Then, $n = 1$ provides the weakest radiofrequency field $B_1 = J_{IS}\sqrt{3}/4$, affording highest ν^I and ν^S frequency selectivity, while the tolerance to relative B_1 miscalibration and mismatch is maximized. The latter collateral benefit of frequency selective hetero-nuclear Hartmann-Hahn transfers crucially important and in stark contrast to its unselective (broadband) implementation, where the exacerbated losses from B_1 mismatch (inevitable for separate probe coils for I and S and scaling with B_1) effectively prevent wider use of the technique in solution state NMR.

To achieve HH-SPT in a ISM three spin system with $J_{IM}=0$ and without decoupling of spin M we introduce a method of the frequency Selective and Spin State Selective Polarisation Transfer $S^4\text{PT}$. If $J_{SM} \approx J_{IS}$, the HH-SPT is possible because the detrimental effect of the passive coupling J_{SM} is efficiently suppressed by using slightly higher CW field B_1 (i.e. $n = 2$ or 3 in Eq. S1) in expense of a small loss of frequency selectivity of the Hartmann-Hahn magnetization transfer. When $J_{SM} > J_{IS}$, the signal of spin S may be “broadened” beyond the extremely narrow HH-SPT bandwidth $\text{BW} \approx B_1 \approx J_{IS}$ (see above) by splitting due to a larger passive coupling J_{SM} . Efficient HH-SPT can then still be achieved by addressing both lines of the S signal doublet separately^{1,2,5} via the same low power CW irradiation (with B_1 given by Eq. S1) at the three frequencies ν^I , $\nu^S - \frac{1}{2}J_{SM}$ and $\nu^S + \frac{1}{2}J_{SM}$. Under these conditions, HH-SPT passes via separate $I_x \rightarrow S_x M_\alpha$ and $I_x \rightarrow S_x M_\beta$ parallel pathways that are immune to J_{SM} coupling evolution and can each be described by the HH-SPT formalism for isolated two spin system.⁴ We use the acronym $S^4\text{PT}$ to refer to such parallel frequency selective and $M_{\alpha/\beta}$ spin state selective polarisation transfer. Importantly, the sign for $S_x M_\alpha$ and $S_x M_\beta$ terms can be controlled via the phase of the pertaining CW irradiation at $\nu^S - J_{SM}/2$ vs. $\nu^S + J_{SM}/2$, where the identical phases lead to $S_x M_\alpha + S_x M_\beta = S_x$ inphase transfer while the opposite phases produce $S_x M_\alpha + S_x M_\beta = 2S_x M_z$ antiphase transfer. The $S^4\text{PT}$ concept can be generalized for spins systems with more than three spins. Specifically, both I and S spins may have passive scalar couplings with several spins. For example, in the HH-SPT $N_x^i \rightarrow C_x^{O,i-1}$, the amide nitrogen of residue i and carbonyl of residue $i-1$ have $^1J_{\text{Ni,Hi}}$ and $^1J_{\text{CO,i-1CA,i-1}}$ large passive couplings, and thus the HH- $S^4\text{PT}$ includes four parallel pathways (i.e. $N_x^i H_\alpha^i \rightarrow C_x^{O,i-1} C_\alpha^{A,i-1}$, $N_x^i H_\alpha^i \rightarrow C_x^{O,i-1} C_\beta^{A,i-1}$, $N_x^i H_\beta^i \rightarrow C_x^{O,i-1} C_\alpha^{A,i-1}$, and $N_x^i H_\beta^i \rightarrow C_x^{O,i-1} C_\beta^{A,i-1}$) and is achieved using CW irradiation at four frequencies $\nu^{\text{CO,i-1}} - \frac{1}{2}J_{\text{CO,i-1CA,i-1}}$ and $\nu^{\text{CO,i-1}} + \frac{1}{2}J_{\text{CO,i-1CA,i-1}}$, $\nu^{\text{Ni,i}} - \frac{1}{2}J_{\text{Ni,Hi}}$ and $\nu^{\text{Ni,i}} + \frac{1}{2}J_{\text{Ni,Hi}}$

LSF- $S^4\text{PT}$

Similar to the PI-SPT described above, for an IS spin system, the Longitudinal Single Field Selective Polarization Transfer module^{4,6} (LSF-SPT) uses a single radiofrequency and thus is frequency selective only for spin I. The LSF-SPT does not depend on frequency

and passive couplings of spin S and it performs efficient transfer of spin I magnetization to antiphase coherence of spin I in respect to spin S ($I_z \rightarrow 2I_x S_z$). The LSF-SPT uses a continuous-wave irradiation of spin I at frequency ν_I with optimal duration $\tau_{CW} = \frac{\sqrt{2}}{2J_{IS}}$

and strengths $B_1 = \frac{J_{IS}}{2}$. Similar to HH-SPT, use of the CW irradiation in the LSF-SPT scheme allows the S⁴PT approach for circumventing the effects of passive scalar couplings of I spin. Thus, for a three spin ISM system with passive couplings $J_{MS}=0$ and $J_{MI} > J_{IS}$, the LSF-S⁴PT with the τ_{CW} and B_1 defined above is performed without decoupling of spin M by two CW's at frequencies $\nu^I - J_{IM}/2$ and $\nu^I + J_{IM}/2$. Transfers $I_z \rightarrow 2I_x S_z$ and $2M_z I_z \rightarrow 2I_x S_z$ are achieved using the CW's aligned at the start with the same and opposite phases, respectively. The LSF-S⁴PT approach can be extended to more passive scalar couplings of spin I by combining the corresponding synphase and antiphase CW's.

The LSF-S⁴PT approach may be illustrated by polarization transfer $2C_z^{A,i-1}C_z^{O,i-1} \rightarrow 2C_x^{A,i-1}N_z^{i-1}$ achieved by applying two radiofrequency CWs at frequencies $\nu^{CA,i-1-1/2}J_{CA,i-1CO,i-1}$ and $\nu^{CA,i-1+1/2}J_{CA,i-1CO,i-1}$ with opposite phases and simultaneous selective $^{13}C^{B,i-1}$ decoupling.⁷ The S⁴PT can be adapted to deal with other passive couplings. For example, without the $^{13}C^{B,i-1}$ decoupling we need four CWs (see Figure S2e) and even the eight CW sandwich for samples having $^1H^{A,i-1}$ atoms (see Figure S3d).

Small ($J_{MI} < J_{IS}$) passive scalar couplings of spin I are taken into consideration by finding optimal τ_{CW} and B_1 values. Specifically, for $2C_z^{A,i-1}C_z^{O,i-1} \rightarrow 2C_x^{A,i-1}N_z^{i-1}$ transfer with active $^1J_{CA,i-1N,i-1} \approx 12$ Hz and passive $^2J_{CA,i-1N,i} \approx 7$ Hz, $\tau_{CW} = 43$ ms and $B_1 = 8$ Hz provide the transfer efficiency of 72% without considering the relaxation, which is similar to the corresponding INEPT efficiency (Fig. S1a, round parentheses). Presence of the smaller two-bond coupling results in back-transfer to $2C_x^{A,i-1}N_z^i$, which is about three times less efficient than the target pathway. Unlike broad-band INEPT, the LSF-SPT block allows even 100% transfer by using the selective decoupling at the known $^{15}N^i$ frequency. However, this may be problematic, since frequencies of $^{15}N^{i-1}$ and $^{15}N^i$ may be close and thus the $^{15}N^i$ decoupling is not used in our experiments.

FOSY experiments

The 2D FOSY ^1H - ^{15}N hnc(CA)NH and ^1H - $^{13}\text{C}^\alpha$ hnc(CA(N))H experiments for deuterated proteins (Figure S1a) start with highly selective population inversion (PI-SPT, Figure S2a) to create ν^{H} frequency selected and γ^{H} enhanced $2H_z^i N_z^i$ two-spin magnetization. Then, a hard 90° pulse on ^{15}N produces anti-phase coherence $2H_z^i N_x^i$ for the subsequent selective Hartmann-Hahn polarisation transfer (HH-S⁴PT) step $2H_z^i N_x^i \rightarrow 2C_x^{O,i-1} C_z^{A,i-1}$. Then, chemical shifts of $^{13}\text{C}^{\alpha,i-1}$ or $^{15}\text{N}^{i-1}$ are traditionally sampled during corresponding constant time periods followed by TROSY $^1\text{H}^{i-1}$ detection.

Figure S1c depicts 2D FOSY hncocacbNH experiment, where the $^{13}\text{C}^{\alpha,i-1}$ constant time INEPT evolution in hnc(CA)NH is replaced by the LSF-S⁴PT module $C_z^{A,i-1} \rightarrow 2C_z^{A,i-1} N_z^{i-1}$. The passive couplings of $^{13}\text{C}^{\alpha,i-1}$ atom are handled by the S⁴PT, i.e. the double continuous-waves at frequencies $\nu^{\text{CA},i-1} - \frac{1}{2} J_{\text{CA},i-1\text{CO},i-1}$ and $\nu^{\text{CA},i-1} + \frac{1}{2} J_{\text{CA},i-1\text{CO},i-1}$ (Figure S2d), and by using the frequency selective decoupling¹⁵ of $^{13}\text{C}^{\beta,i-1}$. The obtained additional frequency selectivity in $^{13}\text{C}^{\beta,i-1}$ makes the effective resolution of the experiment equivalent to a 7D. Although the used strength of the $^{13}\text{C}^{\beta,i-1}$ decoupling of several hundred Hertz, provides relatively low resolution in the $^{13}\text{C}^{\beta,i-1}$ dimension, it is sufficient in most cases to confirm or disprove the type of an amino acid. Since the relatively strong $^{13}\text{C}^{\beta,i-1}$ decoupling field may perturb the $^{13}\text{C}^{\alpha,i-1}$ magnetization, we apply a compensating radiofrequency irradiation at the opposite side of the $^{13}\text{C}^{\alpha,i-1}$ resonance (Figure S2d). If the $^{13}\text{C}^{\beta,i-1}$ frequency is not known, handling of both $^1J_{\text{CA},i-1\text{CO},i-1}$ and $^1J_{\text{CA},i-1\text{CB},i-1}$ passive couplings is included into the S⁴PT irradiation sandwich by performing a 4-frequency CW (qcw6 in Figure S2e) applied simultaneously at all four components of the $C_{\pm}^{A,i-1}$ quartet.

For non-deuterated proteins, the $^2\text{H}^{\alpha,i-1}$ broadband decoupling in the hnc(CA)NH and hnc(CA(N))H experiments (Figure S1a) is replaced by two $^1\text{H}^{\alpha,i-1}$ inversion pulses (Figure S3a). This ensures that the magnetization of water and protein aliphatic protons is returned to the thermal equilibrium state. To adapt the hncocacbNH experiment, we replace the module shown in Figure S1c by the block depicted in Figure S3b. The corresponding LSF-S⁴PT sandwiches with and without $^{13}\text{C}^{\beta,i-1}$ decoupling are depicted in Figure S3c and Figure S3d, respectively. In order to avoid perturbation of the water magnetization, handling of the passive $^1J_{\text{CA},i-1\text{HA},i-1}$ coupling is included into the S⁴PT modules (Figures S3c and S3d).

For Tau, which is an IDP characterized by slow transverse relaxation, $^{15}\text{N}^{\text{H},i}$ frequency selectivity is further improved as shown in Figure S1b. The IP-SPT module is replaced by the initial 90° pulse on $^1\text{H}^{\text{N},i}$ followed by the first magnetization transfer $H_x \rightarrow N_x^i$ performed using the HH-SPT with simultaneously applied CWs at $^1\text{H}^{\text{N},i}$ and $^{15}\text{N}^{\text{H},i}$ frequencies. The subsequent HH-S⁴PT step $N_x^i \rightarrow 2C_x^{O,i-1} C_z^{A,i-1}$ is achieved by applying CW field only at one nitrogen frequency at the position of $^{15}\text{N}^{\text{H},i}$ (scw3) with selective decoupling at the $^1\text{H}^{\text{N},i}$ frequency (scw5). The use of a single cw3 for $^{15}\text{N}^{\text{H},i}$ instead of double cw3 (figure S2b) sandwich results in two times higher nitrogen frequency selectivity, while the selectivity on $^{13}\text{C}^{\text{O},i-1}$ provided by the dual-frequency CW sandwich (dcw4, Figure S2c) is the same as in the original experiment (Figure S1a). Both versions can be used for either deuterated or non-deuterated proteins. The choice between the experiment versions in Figure S1a and Figure S1b exemplifies the versatility of the FOSY approach and the possibility to tailor the experiment to a specific spin system. Namely, while the former version of the experiment reduces relaxation losses and thus prioritizes sensitivity, the latter is resolution optimized.

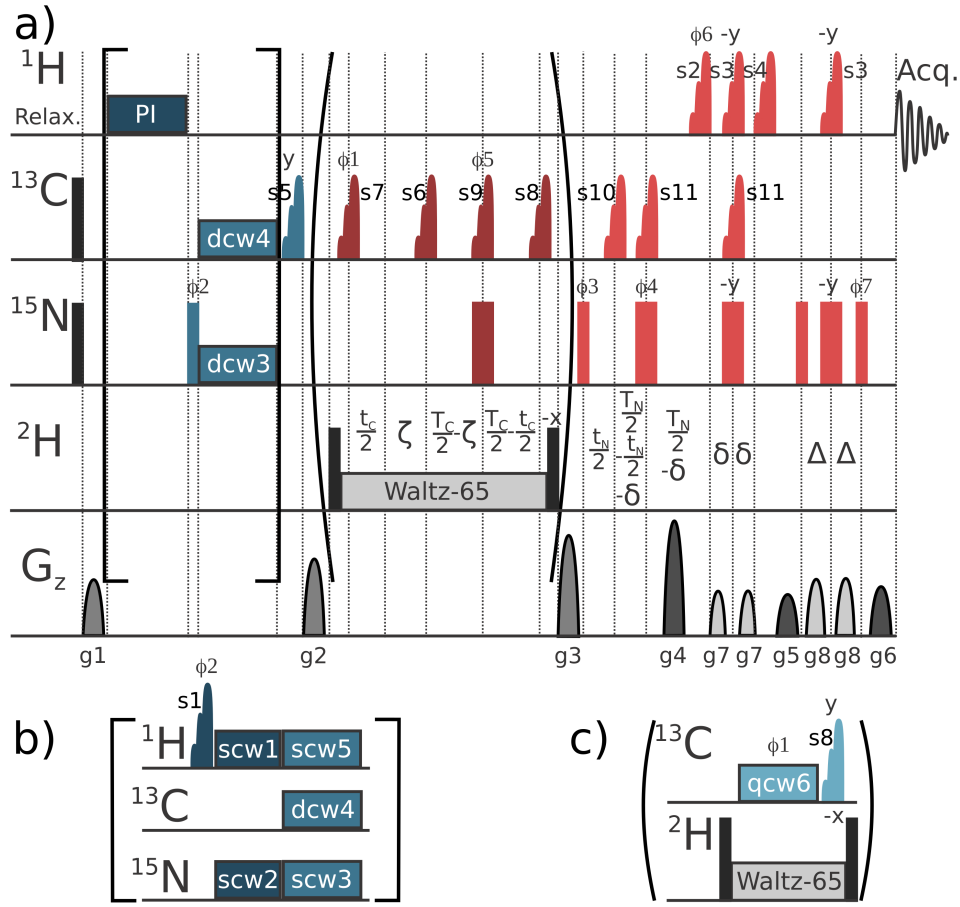


Figure S1. Inter-residual FOSY experiments for deuterated proteins in H_2O -based buffer solution. Selective (PI-SPT, HH-S⁴PT, LSF-S⁴PT) and broadband (INEPT, ST2-PT) polarisation transfer blocks are color-coded in blue and red, respectively, according to Figure 1 in the main text. **a)** The 2D FOSY ^1H - ^{15}N hncoc(CA)NH and ^1H - ^{13}C hncocA(N)H experiments are acquired as the corresponding 2D planes of 3D FOSY-hncocANH experiment depicted in the panel. The selective population inversion (PI) with a CROP-shaped pulse selectively inverts the ^1H TROSY component producing $2H_z^i N_z^i$ polarisation.¹⁻³ The next 90° ^{15}N hard pulse converts it to $2H_z^i N_x^i$ coherence, followed by the HH-S⁴PT block with a double continuous-wave (dcw3, see Fig. S2) for simultaneous transfer of the ^{15}N TROSY and anti-TROSY components without proton decoupling. The transfer (selective for $^{15}\text{N}_{\text{H},i}$ and $^{13}\text{C}_{\text{O},i-1}$) $2H_z^i N_x^i \rightarrow 2C_x^{O,i-1} C_z^{A,i-1}$ is achieved by a 66.7 ms HH-S⁴PT block including the following: double selective at frequencies $^{15}\text{N}_{\text{H},i} \pm 46$ Hz continuous waves (dcw3) with $B_{\text{dcw3}} = 14.5$ Hz beginning at phases $\pm x$; as well as double selective at frequencies $^{13}\text{C}_{\text{O},i-1} \pm 28$ Hz continuous waves (dcw4) with the same $B_{\text{dcw4}} = 14.5$ Hz ending at phases $\pm x$. Constant-time States-TPPI evolution of $^{13}\text{C}_{\text{A},i-1}$ (including ^2H A-decoupling) is implemented with a t_c delay and $\phi 1$. Constant-time Echo-Antiecho $^{15}\text{N}_{\text{H},i-1}$ evolution happens during t_N delay with and simultaneous alteration of three gradients $g4^* \text{EA4}$, $g5^* \text{EA5}$, $g6^* \text{EA6}$ ($\text{EA4} = 1$, 0.8750 ; $\text{EA5} = 0.6667$, 1 ; $\text{EA6} = 1$, 0.6595) and $\phi 6 = y$, $-y$, $\phi 7 = y$, $-y$. The constant-time delays T^c and T^N are 14.3 ms and 20 ms respectively; delays are $\zeta = 1/4 J_{\text{CACO}} = 4.7$ ms and $\Delta = 1/4 J_{\text{NH}} = 2.75$ ms. Narrow and thick bars represent 90° and 180° hard pulses, respectively. s1 is a selective 1 ms Sinc 90° pulse centered at $^1\text{H}_{\text{N},i}$; s2 is a 1.74 ms 90° time-reversed Eburp2 pulse (for all the shaped pulses see review by Lescop et al.⁴); s3 is a 1.85 ms 90° Reburp pulse; s4 is a 1.74 ms 90° Eburp2 pulse. The frequencies of the s2, s3, and s4 pulses are centered in the middle of the amide region, i.e. 8.5 ppm. ^{13}C shaped pulses s5 and s6 are 90° and 180° 600 μs Sinc pulses centered at $^{13}\text{C}_{\text{O},i-1}$; s7 and s8 are 90° 500 μs Q5 and Q5tr pulses, respectively applied at 55 ppm; s9 is a 180° 200 μs Q3 pulse at 39 ppm; s10 is a ^{13}C region inversion 800 μs IBurp1 pulse at 173 ppm; s11 is a ^{13}C region inversion 600 μs IBurp1 pulse at 55 ppm. All gradient pulses have the SMSQ shape and 1 ms length except for $g4$, $g5$, $g6$ (0.5 ms) and $g7$, $g8$ (0.3 ms). Strengths of gradients $g1$ - $g8$ are: 57% , 47% , 37% , -80% , 30% , 30.13% , 15% , and 60% , whereas 100% corresponds to 53.5 G/cm. If not specified, the phase of all shape, cw, and hard pulses is x and the phase cycle employed is: $\phi 1=x, -x$; $\phi 2=2(-y)$, $2(y)$; $\phi 3=4(x)$, $4(-x)$; $\phi 4=8(x)$, $8(-x)$; $\phi 5=16(x)$, $16(-x)$; $\phi 6=y$; $\phi 7=y$; $\phi \text{rec}=4(x - x - x - x - x - x - x)$. **b)** The modification of the pulse program for increasing the selectivity in $^{15}\text{N}_{\text{H},i}$. The shown block in square brackets replaces the corresponding block in the pulse sequence in panel (a). The selective population inversion in panel (a) is replaced with selective 90° s1 pulse followed by the 11 ms HH-SPT block (centered at $^1\text{H}_{\text{N},i}$ and $^{15}\text{N}_{\text{H},i}$) including single-frequency continuous wave (scw1) and scw2 with the same strength $B_{\text{scw1}} = B_{\text{scw2}} = 39$ Hz. Double frequency dcw3 is changed to single frequency scw3 with the same $B_{\text{scw3}} = 14.5$ Hz with the selective continuous-wave decoupling scw5 at $^1\text{H}_{\text{N},i}$ with $B_{\text{scw5}} = 700$ Hz. **c)** 2D FOSY hncocacbNH $^{13}\text{C}_{\text{A},i-1}$ and $^{13}\text{C}_{\text{B},i-1}$ selective modification of the experiment using 59 ms LSF-S⁴PT with quadro-continuous-wave6 (two at $^{13}\text{C}_{\text{A},i-1} \pm 28$ Hz with $B_1 = J_{\text{NCA}}/2 = 6$ Hz and the frequency selective decoupling of $^{13}\text{C}_{\text{B},i-1}$ with corresponding compensation.

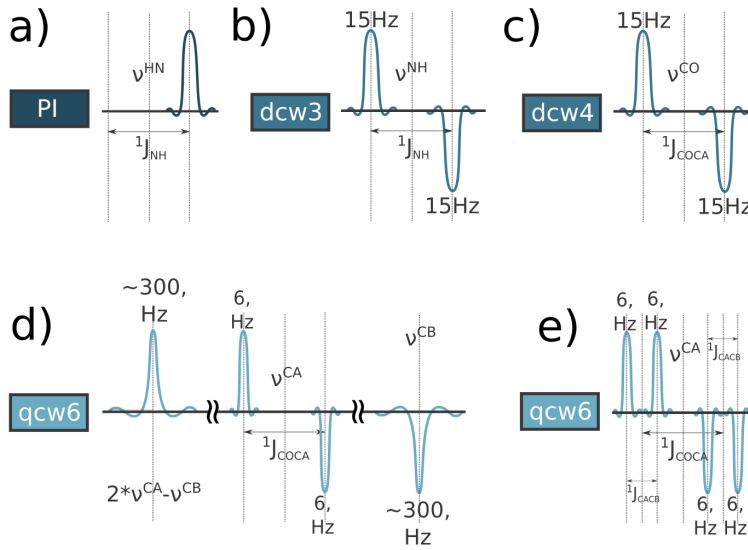


Figure S2. Frequency scheme of the continuous-wave sandwiches used in the FOSY experiment in Figure S1. **a)** Selective single pulse for population inversion of ^1H TROSY component for $H_z^N \rightarrow 2H_z^N N_z^H$ polarization transfer. The pulse may have the Gaussian or CROP shapes. The latter profile is specifically optimized for the cross-correlated relaxation.^{3, 8} **b)** Double continuous-wave sandwich dcw3 includes two continuous-waves with offsets $\nu^{NH} \pm J_{NH}/2$ starting with opposite phases 0, 180 (depicted as shapes pointing up/down). The B_1 strength for the both continuous-waves is 14.5 Hz. **c)** Double continuous-wave sandwich dcw4 includes two continuous-waves with offsets $\nu^{CO} \pm J_{COCA}/2$ finishing with opposite phases. The B_1 strength for both continuous-waves is the same 14.5 Hz. **d)** Quadro continuous-wave sandwich qcw6 for deuterated proteins with $^{13}\text{C}^B$ decoupling includes four continuous-waves: two with $\nu^{CA} \pm J_{COCA}/2$ offsets finishing with the opposite phases, and two decoupling continuous-wave at $^{13}\text{C}^B$ offset ν^{CB} and compensation continuous-wave at $2\nu^{CA} - \nu^{CB}$ with opposite phase. The B_1 strength is 6 Hz for $^{13}\text{C}^A$ continuous-waves. For $^{13}\text{C}^B$ decoupling $J_{CAB} \ll B_1$ the value (e.g. 300 Hz) is selected to match/distinguish different types of amino acid. **e)** Quadro continuous-wave sandwich qcw6 for deuterated proteins without $^{13}\text{C}^B$ decoupling includes four 6 Hz continuous-waves at $\nu^{CA} \pm J_{CACO}/2 \pm J_{CAB}/2$ frequencies finishing at phases 0, 0, 180, and 180.

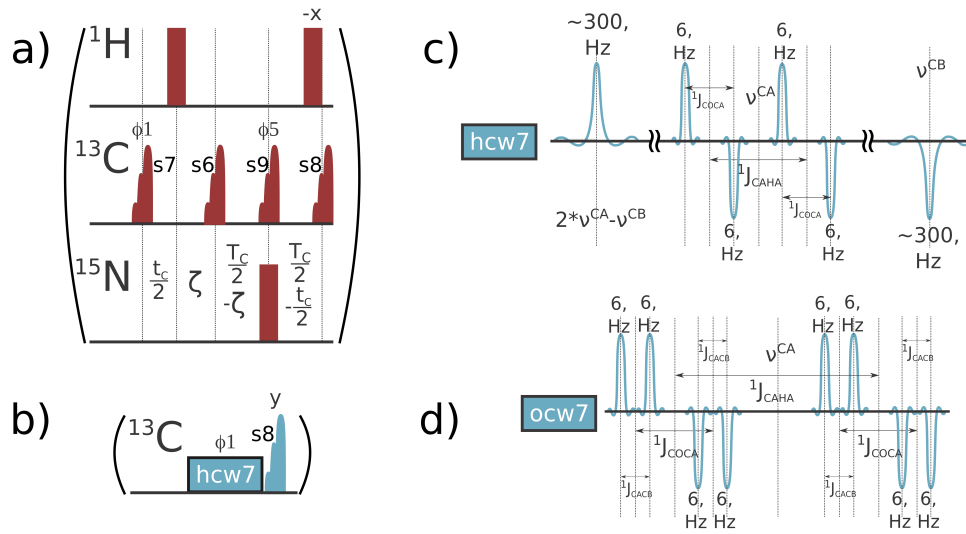


Figure S3. Modification of the experiments shown in Fig. S1 to make them suitable for non-deuterated proteins in H_2O -based buffer. The part in round brackets in Fig. S1 is replaced by a block: **a)** For the 3D pulse sequence (Fig. S1ab), $^2\text{H}^A$ -decoupling is replaced with two 180° inversion ^1H hard pulses. **b)** For the version of the experiment with fixed $^{13}\text{C}^A$ and $^{13}\text{C}^B$ decoupling (Fig. S1c) **c)** The frequency scheme of the hexo continuous-wave sandwich hcw7 with $^{13}\text{C}^B$ decoupling for protonated proteins includes hexo-continuous waves: four 6 Hz continuous-waves at $\nu^{CA} \pm J_{CAHA}/2 \pm J_{CACO}/2$ frequencies finishing with phases 0, 180, 0, and 180 depicted as shapes pointing up (0) and down (180), and decoupling $J_{CAB} \ll B_1 \approx 300\text{Hz}$ continuous wave at $^{13}\text{C}^B$ frequency and compensation continuous-wave at $2\nu^{CA} - \nu^{CB}$ with the opposite phase. **d)** Frequency scheme of the octo-continuous wave sandwich ocw7 for protonated proteins without $^{13}\text{C}^B$ decoupling includes eight 6 Hz continuous waves at $\nu^{CA} \pm J_{CAHA}/2 \pm J_{CACO}/2 \pm J_{CAB}/2$ frequencies finishing at phases 0, 0, 180, 180, 0, 0, 180, and 180.

Proline – Selective Experiments

The triple resonance experiments used in this work are based on BEST-TROSY HNCA and HNcoCA sequences.⁹ To achieve proline selection the sequences are modified according to the approach described by Solyom et al.¹⁰ Thereby the ^{15}N 180° pulse in the middle of the constant time (56 ms) $^{13}\text{C}^{\text{A}}$ chemical shift evolution period t_1 is converted to be band selective using a REBURP shape.¹¹ This pulse is on and off in alternate scans, so that the J_{CANpro} coupling is either evolving (on) or refocused (off). The scans are subsequently subtracted by means of a 180° phase shift of the receiver. In the final spectrum only those peaks are observed, where the $^{13}\text{C}^{\text{A}}$ spin is bound to a $^{15}\text{N}^{\text{H}}$ spin whose chemical shift is within the inversion 250 Hz (138±2.77 ppm) bandwidth of the 8.25 ms REBURP pulse, in the proline region.

Experimental NMR technical details

NMR experiments were performed on a Bruker AVANCE III HD 800 spectrometer equipped with 3 mm TCI $^1\text{H}/^{13}\text{C}/^{15}\text{N}$ cryoprobe. Spectra acquisition, processing, and analysis were performed using TopSpin 3.5 (Bruker BioSpin). 2D FOSY-hncoCA(N)H experiment was recorded as a complex matrix of 150×1024 data points, and 2D FOSY-hnco(CA)NH and 2D FOSY-hncocacbNH experiments were recorded as complex matrixes of 65×1024 data points, with the spectral width of 30 ppm, 26 ppm, and 14 ppm in the indirect ^{13}C and ^{15}N and the direct ^1H dimensions, respectively. The number of scans for each point in the indirect dimension varied from 2 to 32 depending on signal intensity. The proline-selective experiments were recorded for the PX-type as a complex matrix of 128×2048 data points with the spectral width of 26 ppm and 16 ppm in the indirect ^{15}N and direct ^1H dimensions, respectively and for the XP-type as a complex matrix of 64×1024 data points with the spectral width of 41 ppm and 16 ppm in the indirect ^{15}N and direct ^1H dimensions, respectively. The standard 3D BEST-TROSY HNCO experiment from the IBS library¹² was recorded as a complex matrix of 100×100×2048 data points with the spectral width of 10 ppm, 26 ppm, and 16 ppm in the indirect ^{13}C , ^{15}N and direct ^1H dimensions, respectively. A recycle delay of 0.5 s was employed in all experiments.

Protein expression and purification

E. coli BL21(ΔDE3) Star™ (Novagen) cells were transformed with a modified pET28b plasmid harboring full length hTau40 protein fused to an amino-terminal His-SUMO Tag (purchased in *E. coli* codon optimized-form from GenScript). [U - ^{15}N , ^{13}C] or [U - ^2H , ^{15}N , ^{13}C] isotope enriched protein was produced using 2xM9 minimal medium¹³ supplemented with ($^{15}\text{N}^1\text{H}_4$)Cl (1 g/l) and D -(^1H , ^{13}C) or D -(^2H , ^{13}C)-glucose (2 mg/l) as the sole nitrogen and carbon sources, respectively, in either H_2O or D_2O based growth medium. All isotopes were purchased from Merck. The transformed cells were grown at 37°C in medium supplemented with 50 μg/ml kanamycin until an $\text{OD}_{600} \approx 0.8$ was reached. Expression was induced by addition of 1 mM isopropyl-thiogalactoside (IPTG) (Thermo Scientific) for 16 h at 22°C. Cells were harvested by centrifugation (5000xg, 30min) and subsequently resuspended in lysis buffer (20 mM NaPi, 500 mM NaCl, pH7.8). Cells were lysed by four passes through an Emulsiflex C3 (Avestin) homogenizer and the cleared lysate was purified with a 5ml HisTrap HP column (GE Healthcare). hTau40 eluted within a 150 mM imidazole step. Fractions containing hTau40 were pooled and dialyzed overnight, against human SenP1 cleavage buffer (20 mM TrisHCl, 150 mM NaCl, 1 mM DTT, pH 7.8). After dialysis SenP1 protease (Addgene #16356)¹⁴ was added and the enzymatic cleavage was performed for 4 hours at room temperature. Separation of the His-SUMO-Tag and hTau40 was done by a second HisTrap HP column step and fractions containing cleaved hTau40 in the flow-through were collected, concentrated, and subsequently purified by gel filtration using a HiLoad 10/60 200pg (GE Healthcare) pre-equilibrated with NMR buffer (25 mM sodium phosphate buffer pH 6.9, 50 mM NaCl, 1 mM EDTA). The pure hTau40 fractions were concentrated to about 500 μM, flash frozen in liquid nitrogen, and stored at -80°C till usage.

Phosphorylation of Tau protein

GSK3β kinase was purchased from SignalChem. In vitro phosphorylation reactions were carried out as described before.¹⁵ Briefly, 250 μM [U - ^2H , ^{15}N , ^{13}C] hTau40 was mixed with 5 μl of GSK3β in phosphorylation buffer (20 mM HEPES, 2 mM ATP (Thermo Scientific), 25 mM MgSO_4 , 2 mM EDTA, pH 7.4). The reaction was performed at 25°C for 12 hours followed by gel filtration (Superdex® 200 Increase 10/300 GL, GE Healthcare) with NMR buffer. Under the conditions chosen, GSK3β kinase phosphorylated hTau40 to near completion (>95%) as assessed by NMR spectroscopy.

Table S1. Peptide sequence stretches considered by the FOSY assignment strategy, i.e. all those in hTau40 sequence that conform with the general sequence motif (P/G)-Xⁿ-p(S/T)-Xⁿ-(P/G), where X refers to a non-glycine and non-proline residue. The list of peptide stretches is additionally curated using the reported in the literature phosphorylation sites¹⁶ and/or the known kinase consensus sequence motif. Progressing one sequence position at a time, the X amino acid can be classified as preceding a proline (-XP), following a proline (PX-), following a glycine (GX-) or none of the above, ruling out peptide sequences that cannot be mapped based on the derived sequence motif. In case of peaks 'a' and 'd' (Figure S4), after moving backwards 3 and 2 positions respectively, only one peptide sequence stretch matches the derived GXTp(S/T)P and PXXXp(S/T) motifs, indicating pS⁴⁰⁴ and pS⁴⁰⁹ as the phosphorylated residues.

		peak 'a'				peak 'd'			
Tau p-sites by		pos 0	-1	-2	-3	pos 0	-1	-2	-3
GSK3β ¹⁶	Peptide Mapping	(S/T)P	T	X	G	(S/T)	X	X	PX
T175	PAK <u>T</u> P	x		x					
T181	PK <u>T</u> P	x							
S199	GDRSGY <u>S</u> SP	x		x	x				
T205	PG <u>T</u> P	x							
S212	PGSR <u>S</u> RTP	x		x					
S214	P <u>S</u> LP								
T217	P <u>T</u> P								
T231	PKKVAVVR <u>T</u> P	x		x					
S235	PK <u>S</u> P	x							
S262	G <u>S</u> TENLKHQP					x			
S356	G <u>S</u> LDNITHVP					x			
S396	GAEIVYK <u>S</u> P	x		x					
S400	PVV <u>S</u> G					x	x		
S404	GDT <u>S</u> P	x	x	x	x				
S409	PRHL <u>S</u> N					x	x	x	x

Table S2. Obtained in this work chemical shift values (in ppm) for stretch $^{398}\text{VVS}^{\text{GDT}}\text{S}^{404}$ or phosphorylated deuterated [$U\text{-}^2\text{H}, ^{15}\text{N}, ^{13}\text{C}$] ^2H -pTau, and stretch $^{398}\text{VVS}^{\text{GDT}}\text{T}^{403}$ for unphosphorylated deuterated [$U\text{-}^2\text{H}, ^{15}\text{N}, ^{13}\text{C}$] ^2H -Tau and unphosphorylated protonated [$U\text{-}^{15}\text{N}, ^{13}\text{C}$] ^1H -Tau samples. The assignment was obtained using a 3D BEST-TROSY HNC O^{12} and the frequency-selective 2D FOSY hnc $\text{O}(\text{CA})\text{NH}$ and hnc $\text{O}(\text{CA})(\text{N})\text{H}$ pulse sequences for deuterated (Figure S1) and protonated (Figure S3) protein samples, respectively. The assignment walk was initiated from the newly appeared pS^{404} peak for the ^2H -pTau sample, whereas for the unphosphorylated ^2H -Tau and ^1H -Tau the T^{403} peak was used with values taken from published assignment.¹⁷

		^2H -pTau	^2H -Tau	^1H -Tau
Ser-404	$^1\text{H}^{\text{N}}$	8.43		
	$^{15}\text{N}^{\text{H}}$	120.6		
Thr-403	$^{13}\text{C}^{\text{O}}$	174.2		
	$^{13}\text{C}^{\text{A}}$	61.1		
	$^1\text{H}^{\text{N}}$	7.92	8.00	8.00
Asp-402	$^{15}\text{N}^{\text{H}}$	114.1	114.7	114.8
	$^{13}\text{C}^{\text{O}}$	176.3	176.6	176.6
	$^{13}\text{C}^{\text{A}}$	53.9	53.8	54.2
	$^1\text{H}^{\text{N}}$	8.08	8.06	8.06
Gly-401	$^{15}\text{N}^{\text{H}}$	120.8	120.8	121.0
	$^{13}\text{C}^{\text{O}}$	173.7	173.6	173.7
	$^{13}\text{C}^{\text{A}}$	44.7	44.7	45.1
	$^1\text{H}^{\text{N}}$	8.27	8.27	8.28
Ser-400	$^{15}\text{N}^{\text{H}}$	111.6	111.6	111.8
	$^{13}\text{C}^{\text{O}}$	174.8	174.8	174.8
	$^{13}\text{C}^{\text{A}}$	57.8	57.7	58.2
	$^1\text{H}^{\text{N}}$	8.27	8.25	8.26
Val-399	$^{15}\text{N}^{\text{H}}$	120.4	120.3	120.6
	$^{13}\text{C}^{\text{O}}$	176.0	176.0	176.0
	$^{13}\text{C}^{\text{A}}$	61.4	61.4	61.8
	$^1\text{H}^{\text{N}}$	8.11	8.12	8.12
Val-398	$^{15}\text{N}^{\text{H}}$	125.3	125.3	125.6
	$^{13}\text{C}^{\text{O}}$	176.2	176.2	176.2
	$^{13}\text{C}^{\text{A}}$	61.8	61.8	62.3
	$^1\text{H}^{\text{N}}$	8.00	8.00	8.01
	$^{15}\text{N}^{\text{H}}$	121.4	121.4	121.6

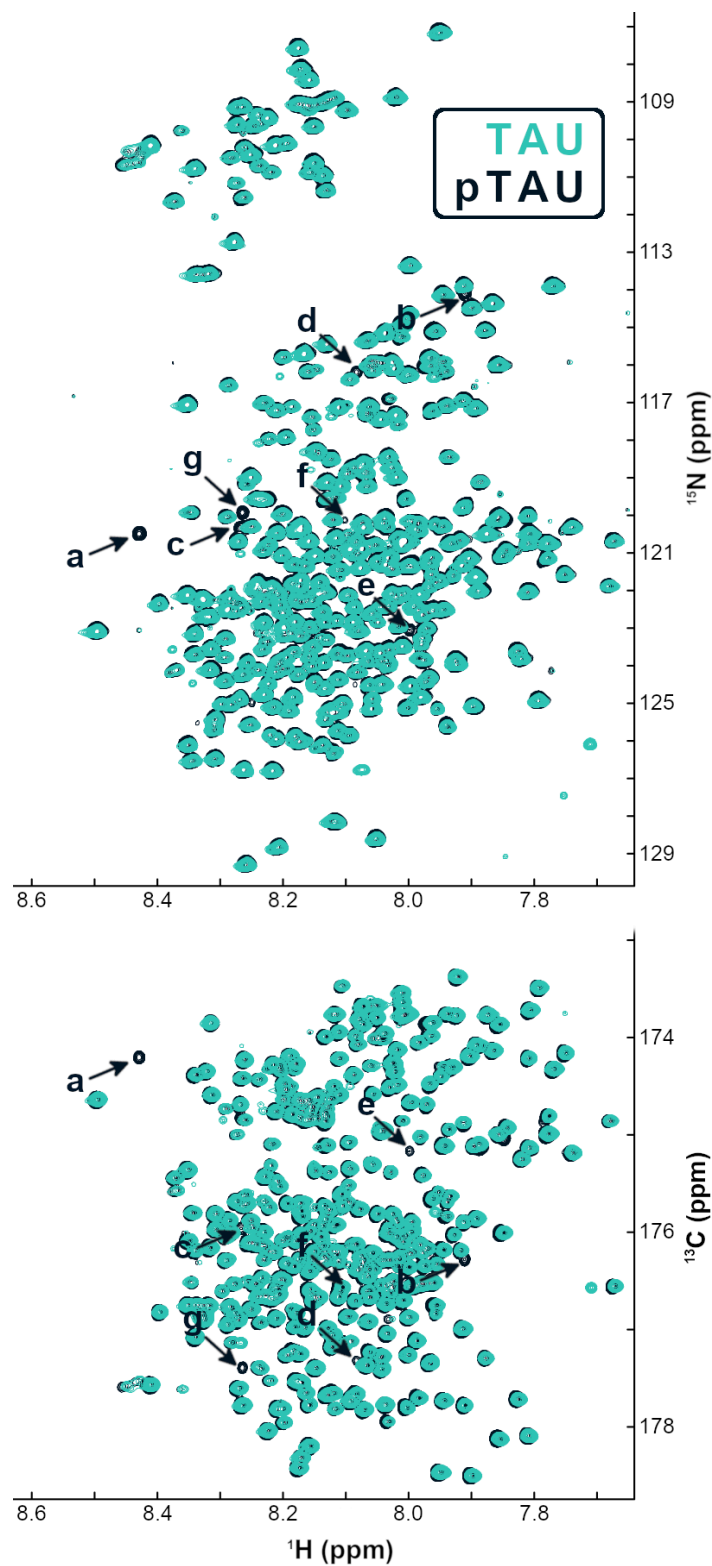


Figure S4. $^1\text{H}/^{15}\text{N}$ (top) and $^1\text{H}/^{13}\text{C}'$ (bottom) projections of 3D BEST-TROSY HNCO¹² of unphosphorylated ^2H -Tau (cyan) and phosphorylated ^2H -pTau (black) samples. All identified new and shifted chemical shifts are annotated with letters a–g. Peaks a, b and c were mapped on the pS⁴⁰⁴ peptide stretch whereas peaks d, e, f and g were mapped on the pS⁴⁰⁹ stretch.

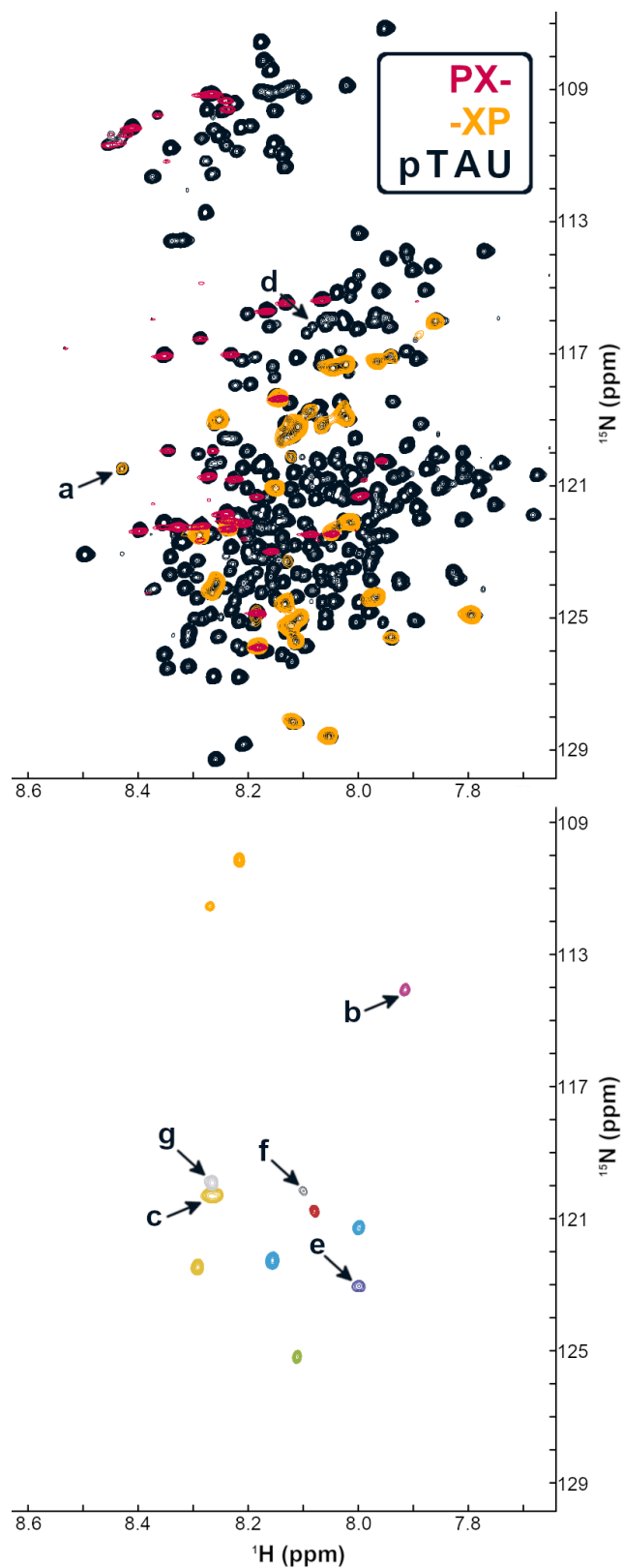


Figure S5. (top) Overlay of 2D $^1\text{H}/^{15}\text{N}$ Pro-selective experiments (for PX-type residues in red and for XP-type residues in yellow) on the corresponding projection of 3D BEST-TROSY HNCO experiment of ^2H -pTau. Annotated a and d peaks were the starting points for the assignment of the two phosphorylation sites. **(bottom)** Overlay of all nine 2D FOSY-hnco(CA)NH experiments performed to identify the new and shifted peaks b-c and e-g that were mapped in the two stretches, respectively. Each individual spectrum is coloured differently, using the same colour for multiple peaks appearing in a single spectrum.

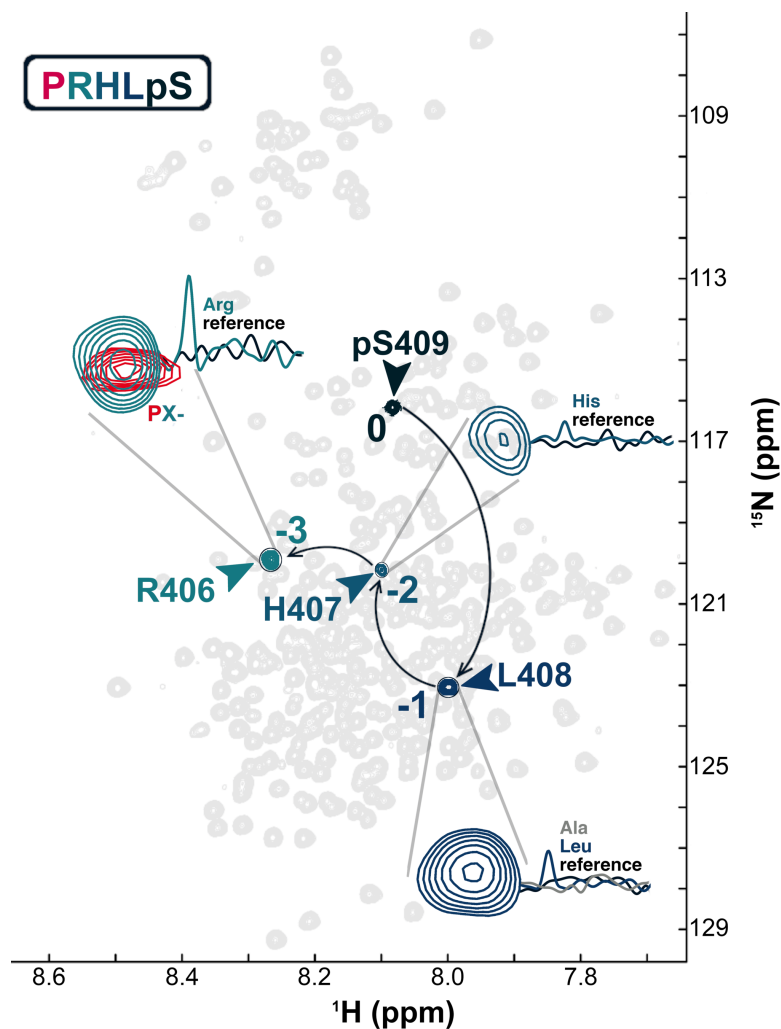


Figure S6. Assignment of the second phosphorylation site in ^2H -pTau with the FOSY assignment strategy. Step-by-step ‘walking’ with the 2D FOSY $\text{hnc}(\text{CA})\text{NH}$ and $\text{hnc}(\text{CA})\text{H}$ experiments from peak 0 (peak ‘d’ in the HNCO spectrum in Figure S4) to peak -1, peak -2, and on until a PX- or GX- type residue is identified created the PXXXp(S/T) motif, that is mapped to three peptide stretches PQLAT⁴²⁷, PVDLS³¹⁶, PRHLS⁴⁰⁹ in the Tau primary sequence. The FOSY- $\text{hnc}(\text{CA})\text{NH}$ is used to determine residue types, i.e. discriminate between Ala and Leu for peak -1, and confirm His for peak -2 and arginine for peak -3. We therefore identify the pS⁴⁰⁹ site, which not surprisingly, is in the only stretch shortlisted as a known GSK3 β -mediated phosphorylation site in Table S1, while the sites in the other two stretches are not.

REFERENCES

1. Sørensen, S.; Hansen, R.; Jakobsen, H., Assignments and relative signs of ^{13}C -X coupling constants in ^{13}C FT NMR from selective population transfer (SPT). *J. Magn. Reson.* **1974**, *14* (2), 243-245.
2. Pachler, K.; Wessels, P., Sensitivity gain in a progressive-saturation selective population inversion NMR experiment. *J. Magn. Reson.* **1977**, *28* (1), 53-61.
3. Khaneja, N.; Luy, B.; Glaser, S. J., Boundary of quantum evolution under decoherence. *PNAS* **2003**, *100* (23), 13162-13166.
4. Pelupessy, P.; Chiarparin, E., Hartmann-Hahn polarization transfer in liquids: an ideal tool for selective experiments. *Concepts Magn. Reson.* **2000**, *12* (3), 103-124.
5. Konrat, R.; Zieger, G.; Sterk, H.; Bermel, W., Specific spin-state transformations induced by amplitude-modulated RF pulses. *J. Magn. Reson., Ser A* **1994**, *106* (1), 23-31.
6. Rey Castellanos, E. R.; Frueh, D. P.; Wist, J., Selective polarization transfer using a single rf field. *J. Chem. Phys.* **2008**, *129* (1), 07B602.
7. Huth, J.; Bodenhausen, G., Suppression of passive scalar couplings in doubly selective coherence transfer. *J. Magn. Reson., Ser A* **1995**, *114* (1), 129-131.
8. Stefanatos, D.; Glaser, S. J.; Khaneja, N., Relaxation-optimized transfer of spin order in Ising spin chains. *Phys. Rev. A* **2005**, *72* (6), 062320.
9. Lescop, E.; Kern, T.; Brutscher, B., Guidelines for the use of band-selective radiofrequency pulses in hetero-nuclear NMR: example of longitudinal-relaxation-enhanced BEST-type ^1H - ^{15}N correlation experiments. *J. Magn. Reson.* **2010**, *203* (1), 190-198.
10. Solyom, Z.; Schwarten, M.; Geist, L.; Konrat, R.; Willbold, D.; Brutscher, B., BEST-TROSY experiments for time-efficient sequential resonance assignment of large disordered proteins. *J. Biomol. NMR* **2013**, *55* (4), 311-21.
11. Geen, H.; Freeman, R., Band-selective radiofrequency pulses. *J. Magn. Reson.* **1991**, *93* (1), 93-141.
12. Favier, A.; Brutscher, B., NMRlib: user-friendly pulse sequence tools for Bruker NMR spectrometers. *J. Biomol. NMR* **2019**, *73* (5), 199-211.
13. Azatian, S. B.; Kaur, N.; Latham, M. P., Increasing the buffering capacity of minimal media leads to higher protein yield. *J. Biomol. NMR* **2019**, *73* (1-2), 11-17.
14. Mikolajczyk, J.; Drag, M.; Békés, M.; Cao, J. T.; Ronai, Z. e.; Salvesen, G. S., Small ubiquitin-related modifier (SUMO)-specific proteases: profiling the specificities and activities of human SENPs. *J. Biol. Chem.* **2007**, *282* (36), 26217-26224.
15. Burmann, B. M.; Gerez, J. A.; Matečko-Burmann, I.; Campioni, S.; Kumari, P.; Ghosh, D.; Mazur, A.; Aspholm, E. E.; Šulskis, D.; Wawrzyniuk, M., Regulation of α -synuclein by chaperones in mammalian cells. *Nature* **2020**, *577* (7788), 127-132.
16. Rankin, C. A.; Sun, Q.; Gamblin, T. C., Tau phosphorylation by GSK-3 β promotes tangle-like filament morphology. *Mol. Neurodegener.* **2007**, *2*, 12.
17. Narayanan, R. L.; Dürr, U. H.; Bibow, S.; Biernat, J.; Mandelkow, E.; Zweckstetter, M., Automatic assignment of the intrinsically disordered protein Tau with 441-residues. *J. Am. Chem. Soc.* **2010**, *132* (34), 11906-11907.